Journal of Applied Polymer Science

Preparation, Characterization, and Properties of Modified Barium Sulfate Nanoparticles/Polyethylene Nanocomposites as T-Shaped Copper Intrauterine Devices

Xiuxiang Cao,[1] Han Zhang,[1] Minfang Chen,[1,2] Liang Wang[2]

[1]School of Materials Science and Engineering, Tianjin University of Technology, Tianjin 300384, China

[2]Key Laboratory of Display Materials & Photoelectric Devices (Tianjin University of Technology), Ministry of Education, Tianjin 300384, China

Correspondence to: M. Chen (E-mail: mfchentj@126.com)

ABSTRACT: To improve the mechanical properties and shelf-life of barium sulfate nanoparticles ($BaSO_4$-NPs)/polyethylene (PE) composites, which are used as the scaffold of T-shaped copper intrauterine devices (Cu-IUDs) in the clinic, an Al coupling agent was used to modify $BaSO_4$-NPs. The influence of the Al coupling agent on the microstructures, properties, and shelf-life of the nanocomposites were investigated. The results showed that: (1) a chemical reaction occurred between the Al coupling agent and the hydroxyl groups adsorbed by $BaSO_4$-NPs. (2) $BaSO_4$-NPs modified by the Al coupling agent dispersed in the PE matrix were much better than unmodified NPs. The interface bonding between modified NPs and the PE matrix was better than unmodified NPs. (3) the maximum tensile strength of nanocomposites containing modified NPs was 11.87 MPa, flexural strength was 6.61 MPa, and the elongation rate was 66.78%. (4) After an accelerated aging experiment, the tensile strength of the nanocomposites only decreased 5–15%. All of these results indicate that m-$BaSO_4$-NPs/PE nanocomposites are more clinically useful than unmodified nanocomposites. © 2014 Wiley Periodicals, Inc. J. Appl. Polym. Sci. **2014**, *131*, 40393.

KEYWORDS: biodegradable; biomedical applications; biomaterials

Received 6 September 2013; accepted 4 January 2014
DOI: 10.1002/app.40393

INTRODUCTION

T-shaped copper intrauterine devices (Cu-IUDs) are a form of reversible contraception for birth control,[1–4] usually supported by a T-shaped plastic scaffold of PE composites. The contraceptive effect of such devices depends on the position of the Cu-IUD in the uterus.[5] In the clinic, the position of a Cu-IUD is checked by X-ray. Thus, the scaffold materials (PE composites) are required to be opaque to X-rays so that the position of the Cu-IUD can be determined by X-ray imaging. Because polymers are transparent to X-rays,[6–9] rigid X-ray-opaque inorganic particles are often used in polymers as reinforcement elements and media for developing X-ray images. $BaSO_4$-NPs have excellent acid and alkali resistance,[10–12] as well as a strong toughening effect on low density PE, and are therefore a good reinforcement addition to polymers. Indeed, $BaSO_4$ forms X-ray-opaque rigid inorganic particles,[13] so $BaSO_4$-NPs/polymer composites with low density, low thermal conductivity, and X-rays opacity have been used as materials for the T-shaped plastic scaffold for Cu-IUDs and have been applied in the clinic. Wang *et al.*[14] proposed a method to pretreat $BaSO_4$-NPs with 1 wt % stearic acid and 1 wt % silane AMPTES to improve interfacial adhesion and control the interfacial de-bonding between the PE matrix and $BaSO_4$-NPs. As a result, the PE is simultaneously toughened and reinforced by incorporating $BaSO_4$-NPs. Xu *et al.*[15] prepared a polyvinyl chloride/$BaSO_4$ nanocomposite by means of melt-mixing, demonstrating a promising prospective for synthesizing $BaSO_4$ polymer nanocomposites.

However, NPs are prone to aggregation because of their high surface area-to-volume ratio. Thus, it is difficult to produce a true dispersion of NPs in the polymer matrix.[16] To improve the affinity and adhesion between $BaSO_4$-NPs and the polymer matrix, Al coupling agents had been employed in the synthesis of $BaSO_4$- NPs.[17] In general, coupling agents can modify surface properties of NPs in small quantities such that interfacial energies are reduced and bonding can occur more easily between the surfaces concerned.

The present work aimed to understand the influence of Al coupling agent modification on the surface of $BaSO_4$-NPs and on the performance of $BaSO_4$-NPs/PE nanocomposites, including improving the dispersion of $BaSO_4$-NPs in the PE matrix and

enhancing the thermal and mechanical properties of the material. The mechanisms of the Al coupling agent-assisted surface modification of $BaSO_4$-NPs were investigated, together with the effect of $BaSO_4$-NPs on the properties of the PE matrix nanocomposites.

EXPERIMENTAL

Materials

A commercial PE (MFR = 2.1–2.2 g/10 min), supplied by Beijing Petrochemical, China, was used in the present study. The materials for synthesizing $BaSO_4$-NPs were dihydrate barium chloride [$BaCl_2 \cdot 2H_2O$], anhydrous sodium sulfate [Na_2SO_4], and disodium ethylene diamine tetraacetic acid [Na_2H_2Y] (EDTA). Deionized water was used in the preparation of both chemical solutions and particles suspensions. The Al coupling agent [$(C_3H_7O)_x$ Al-$(COO\text{-}R_1)_m$ $(COO\text{-}R_2)_n$ $(OAB)_y$] was applied to modify the $BaSO_4$-NPs surface. It was purchased from the Nanjing Shuguang Chemical (type DL-411-A).

Synthesis of $BaSO_4$-NPs Suspensions

$BaSO_4$-NPs suspensions were synthesized by mixing 0.6 mol/L Na_2SO_4 and 0.6 mol/L $BaCl_2$ solutions. The complexing agent was 0.6 mol/L EDTA solution. The EDTA solution was added drop wise to 0.6 mol/L $BaCl_2$ solution with vigorous stirring. The pH of the solutions was adjusted to 6.0 using an ammonia solution at 45°C. Then, the 0.6 mol/L Na_2SO_4 solution was added drop wise to the blended solution. The suspension was continuously stirred for 30 min, and then, the suspension was incubated for another 30 min to allow the precipitate to settle. The idealized stoichiometric equation is as follows[18]:

$$Ba^{2+} + H_2Y^{2-} \rightarrow [BaY]^{2-} + 2H^+ \quad < \text{first step} >$$

$$[BaY]^{2-} + SO_4{}^{2-} \rightarrow BaSO_4 \downarrow + Y^{4-} \quad < \text{second step} >$$

The precipitate was then separated, centrifuged, rinsed with deionized water three times, and then dried at 70°C for 24 h in a dryer to obtain dried m-$BaSO_4$-NPs.

Surface Modification of $BaSO_4$-NPs

The Al coupling agent and $BaSO_4$-NPs were separately mixed with 100 ml of toluene. The Al coupling agent solution was added drop wise to the $BaSO_4$-NPs suspension with vigorous stirring at 85°C. The mixture was stirred for another 30 min, and then incubated without stirring to allow reactions between the Al coupling agent and $BaSO_4$-NPs to occur. The m-$BaSO_4$-NPs were then filtered and washed with toluene, followed by ethanol rinsing to remove any trace of Al coupling agent before drying in an oven at 70°C for 24 h.

Preparation of $BaSO_4$-NPs/PE and m-$BaSO_4$-NPs/PE Nanocomposites

$BaSO_4$-NPs and m-$BaSO_4$-NPs (20 wt %) were mixed in the PE matrix using Pentaerythritol Tetrakis [3-(3, 5-di-tert-butyl-4-hydroxyphenyl) propionate] as a stabilizer in a high-speed stirring kneader, followed by melt-blended using a double-roll mixing machine at a rotation speed of 50 rpm at 180°C for 10 min. $BaSO_4$/PE nanocomposite samples of $\sim 80 \times 10^4$ mm^3 were prepared by mold forming using a single-screw injection molding machine.

Accelerated-Aging Experiments

Accelerated-aging experiments for the 20 wt % m-$BaSO_4$-NPs/PE nanocomposites, which contained different contents of Al coupling agent, were performed in a simulated uterine fluid (pH = 7.2) at 90°C. The simulated uterine fluid solution was 4.97 g/L NaCl, 0.224 g/L KCl, 0.167 g/L $CaCl_2$, 0.250 g/L $NaHCO_3$, 0.500 g/L glucose, 0.072 g/L $NaH_2PO_4.2H_2O$, and 0.500 g/L human serum albumin.

Characterization

X-ray diffraction (XRD, Rigaku D/max/2500PC Japan) measurements were performed at room temperature using graphite-monochromatized Cu Kα radiation ($\lambda = 0.1542$ nm). The 2θ angle range was from 10° to 80°. The $BaSO_4$-NPs, m-$BaSO_4$-NPs, PE, PE/20 wt % $BaSO_4$-NPs and 20 wt % m-$BaSO_4$-NPs/PE nanocomposites specimens were examined by a scanning electron microscope (JEOL 6700F, Japan) operated at 10 kV. The interaction between the $BaSO_4$-NPs and the modifier, Al coupling agent, was analyzed by Fourier transform infrared spectroscopy (FT-IR) (560E.S.P, USA). First, a few $BaSO_4$-NPs, m-$BaSO_4$-NPs, and Al coupling agent were separately treated in a vacuum drying oven at 80°C for 24 h. Second, a few $BaSO_4$-NPs, m-$BaSO_4$-NPs, and Al coupling agent were separately ground with potassium bromide in a mortar. Last, the mixed powder was separately pressed into sheets using a tablet press. The sheets were used for FTIR measurement with a 560E.S.P. A Japanese Rugaku analyzer was used for differential scanning calorimetry (DSC). Samples were incubated at 180°C for 5 min to remove their thermal history and then cooled at a rate of 10°C/min to room temperature. The crystallization and melting parameters were obtained from the cooling and heating scans. A thermo gravimetric analysis (TG) was performed with the same Rugaku analyzer, in which samples were heated from 40°C to 800°C at a rate of 20°C/min under nitrogen. Tensile and flexural strength were tested on a CMT-6104 tensile machine. The nanocomposite materials have three parallel samples in each percentage.

RESULTS AND DISCUSSION

Figure 1 shows the XRD patterns of $BaSO_4$-NPs, m-$BaSO_4$-NPs, PE, and 20 wt % m-$BaSO_4$-NPs/PE nanocomposites. The diffraction peaks of $2\theta = 25.84°$, 26.84°, 28.75°, 31.52°, 32.72°, and 42.91° are the characteristic peaks of orthorhombic $BaSO_4$ crystals The diffraction peaks of planes (101), (111), (021), (121), (140), (002), and (211) are the characteristic peaks of orthorhombic $BaSO_4$ crystals. All of the diffraction peaks were able to be indexed with reference to the unit cell of the barite structure (JCPDS card: 24–1035). These results confirmed that the synthesized $BaSO_4$-NPs had a standard $BaSO_4$ crystal structure. The XRD revealed that both $BaSO_4$-NPs and m-$BaSO_4$-NPs were orthorhombic. The diffraction peaks of $2\theta = 21.38°$ and 23.84° are the characteristic peaks of PE. The diffraction peaks of m-$BaSO_4$-NPs were higher than pure $BaSO_4$-NPs, resulting from the interactions with the Al coupling agent.

The size, shape, and collective configurations of the $BaSO_4$-NPs and m-$BaSO_4$-NPs are shown in Figure 2. As can be seen in Figure 2(a), the particles were spherical, with an average

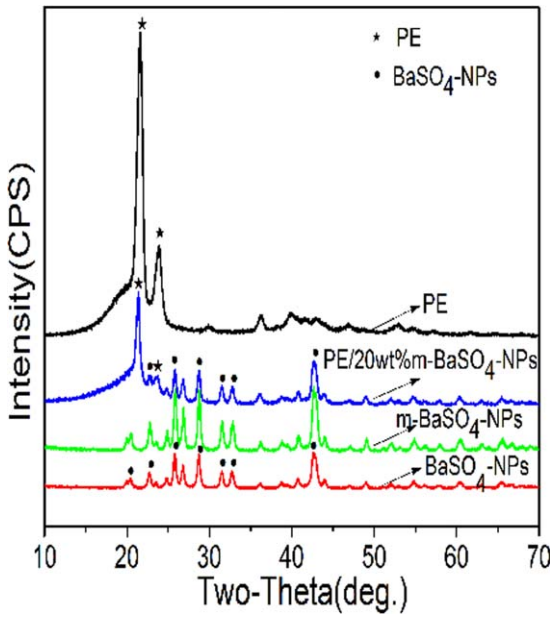

Figure 1. XRD patterns of unmodified $BaSO_4$-NPs, m-$BaSO_4$-NPs, PE, and 20 wt % m-$BaSO_4$-NPs/PE nanocomposites. [Color figure can be viewed in the online issue, which is available at wileyonlinelibrary.com.]

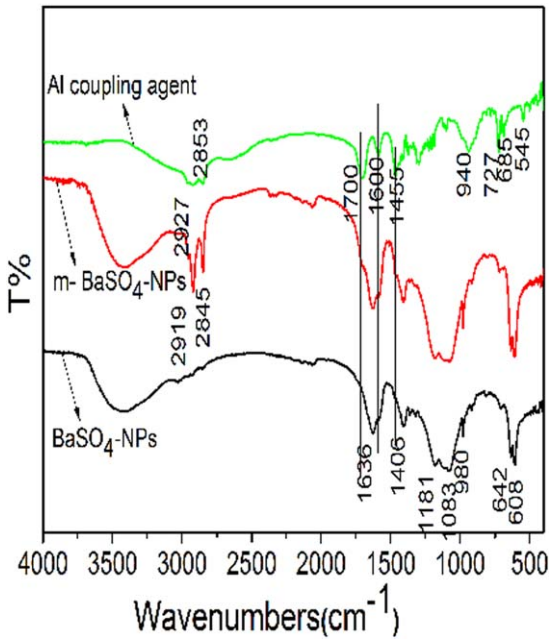

Figure 3. FT-IR of $BaSO_4$-NPs, Al coupling agent, and m-$BaSO_4$-NPs. [Color figure can be viewed in the online issue, which is available at wileyonlinelibrary.com.]

diameter of approximately 50 nm. The m-$BaSO_4$-NPs in Figure 2(b) were also spherical but with an average diameter of ~100 nm.

It is known that PE is nonpolar, whereas $BaSO_4$-NPs are polarized. Therefore, surface modifier can be used on $BaSO_4$-NPs to improve their chemical affinity with PE. Figure 3 shows the FT-IR of $BaSO_4$-NPs, m-$BaSO_4$-NPs, and Al coupling agent. The bands centered at 1636, 1181, 1083, and 980 cm^{-1} are the symmetrical vibrations of SO_4^{2-}. The peaks at 608 and 642 cm^{-1} correspond to the out-of-plane bending vibration of the SO_4^{2-}. The peaks at 545 and 685 cm^{-1} correspond to the symmetric stretching vibrations of the -Al-O group. The 940 cm^{-1} peak was attributed to the presence of an Al-O-C group. The peaks at 1455, 1600, and 1700 cm^{-1} were assigned to the symmetric and asymmetric vibrations of O-C=O. The peaks at 1455, 1600, and 1706 cm^{-1} of the Al coupling agent were not observed. Instead, a new peak at 1648 cm^{-1} was found. The peaks at 2845 and 2919 cm^{-1} were assigned to the symmetric and asymmetric stretching vibrations of $-CH_2-$ and $-CH_3-$ groups. All of these results demonstrated that chemical reactions likely occurred between the Al coupling agent and the $BaSO_4$-NPs.

Scanning electron micrographs (SEM) of the nitrogen brittle section of PE, 20 wt % $BaSO_4$-NPs/PE, and 20 wt % m-$BaSO_4$-NPs/PE nanocomposites are shown in Figure 4. The fracture surface of PE without reinforcement additions was smooth

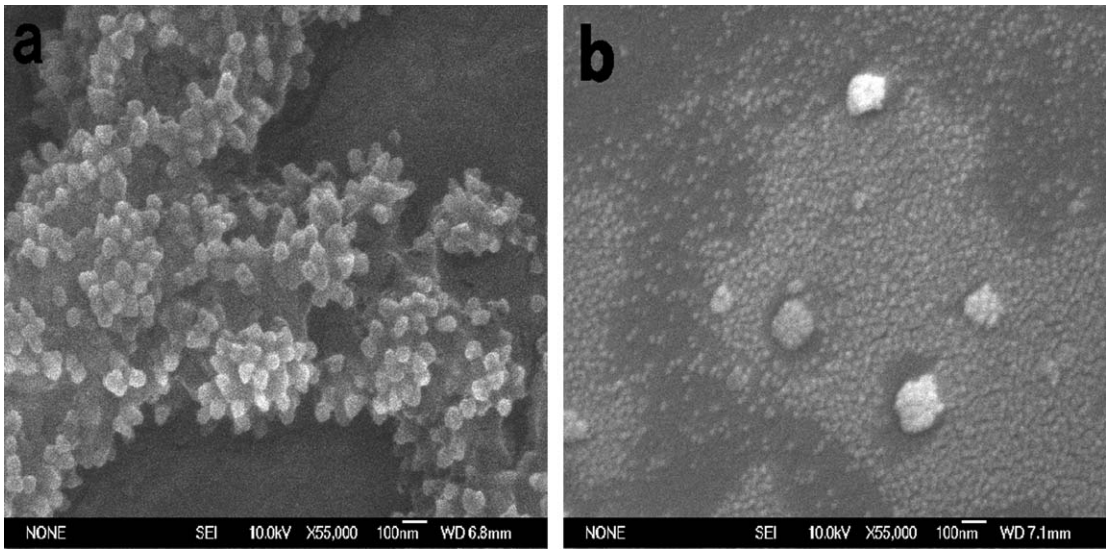

Figure 2. SEM micrographs of $BaSO_4$-NPs and m-$BaSO_4$-NPs.

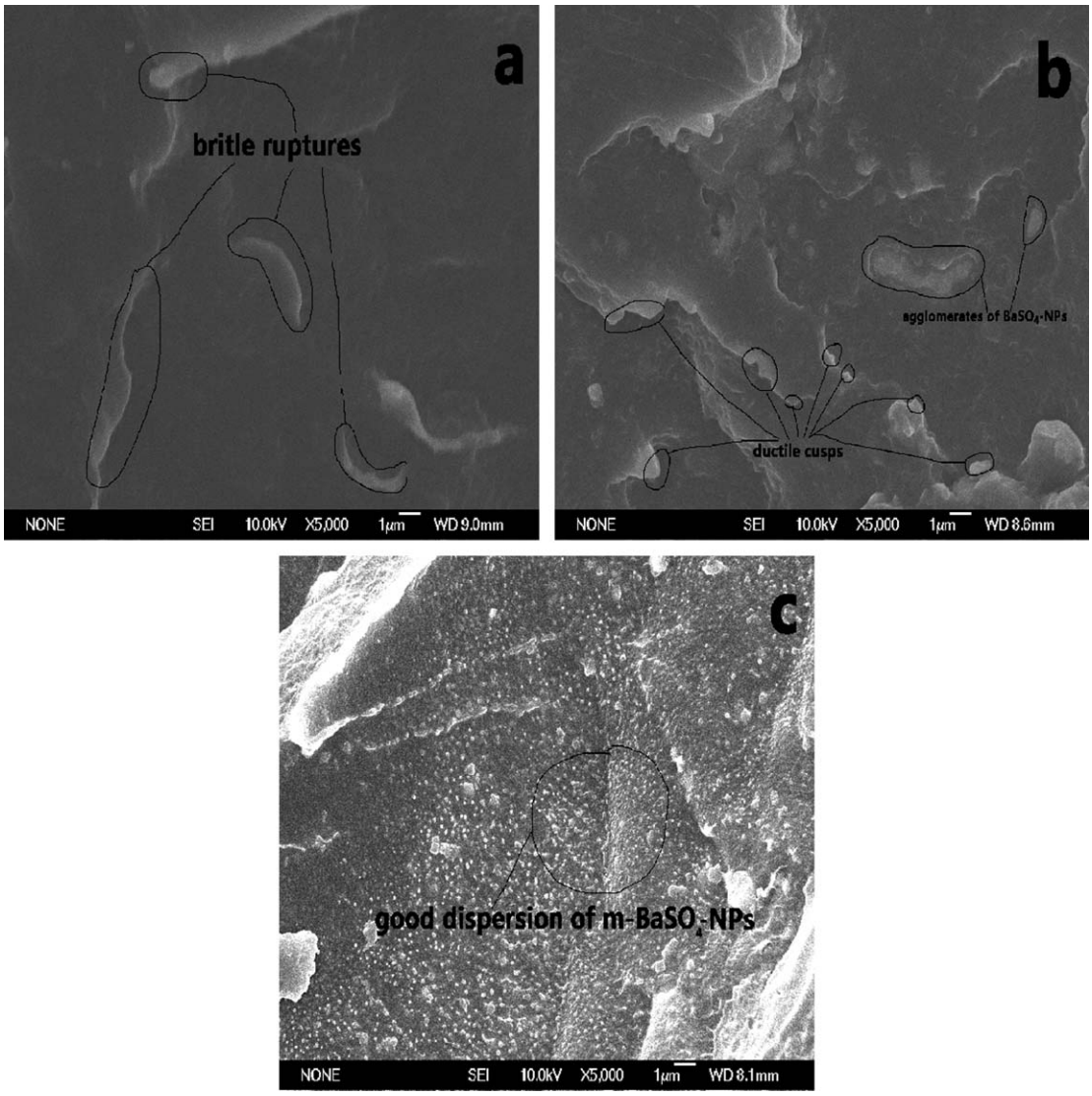

Figure 4. SEM and SEM-EDX photographs of nanocomposites: (a) PE, (b) 20 wt % $BaSO_4$-NPs/PE, and (c) 20 wt % m-$BaSO_4$-NPs/PE.

[Figure 4(a)], showing some brittle nature of rupture. In contrast, the fracture surface of the 20 wt % $BaSO_4$-NPs/PE nanocomposites was rough with ductile cusps [Figure 4(b)]. The size of the aggregates was in the range of 0.5–5 μm. It appeared that the surface energy of the unmodified particles was very high, with a strong tendency to agglomerate to reduce the total surface energy. In fact, Figure 2 shows that unmodified particles remained in aggregates, whereas the modified particles were randomly spaced with limited segregation. We also observed that the interface between unmodified $BaSO_4$-NPs and PE was sharp, suggesting that the interfacial adhesion was poor. In contrast, m-$BaSO_4$-NPs dispersed well in the PE matrix, as shown in Figure 4(c). The interfacial adhesion between the modified nanoparticles and the PE matrix looks substantially improved because of the bridge link of Al coupling agent, though more evidence is needed to confirm this.

As a summary of the abovementioned results, the preparation of m-$BaSO_4$-NPs/PE nanocomposites occurred via three major steps, as shown in Scheme 1: (1) the R_1O-inorganic groups of the Al coupling agent, which are easy to hydrolyze, react with –O-H groups adsorbed by the surface of $BaSO_4$-NPs to produce irreversible Al-O chemical bonds. The packaging was a monomolecular layer, so the modification effect was ideal. (2) The -OR_2 organophilic groups may crosslink with the winding PE molecular chains, and the Al coupling agent connected $BaSO_4$-NPs to PE to form similar bridge connections. Thus, the processing performance, physical properties, and mechanical properties of $BaSO_4$-NPs/PE composites were significantly improved. (3) The Al coupling agent improved the affinity and dispersion between $BaSO_4$-NPs and PE. $BaSO_4$-NPs in the PE matrix agglomerated, whereas m-$BaSO_4$-NPs were well dispersed in the PE matrix. The Al coupling agent was combined tightly with the surface of the $BaSO_4$-NPs. Therefore, during the machining process, the composites avoided exposing polar surfaces because of high temperature and high shear force, which led to poor rheology and processing difficulties. However, modifying $BaSO_4$-NPs with the Al coupling agent avoided the

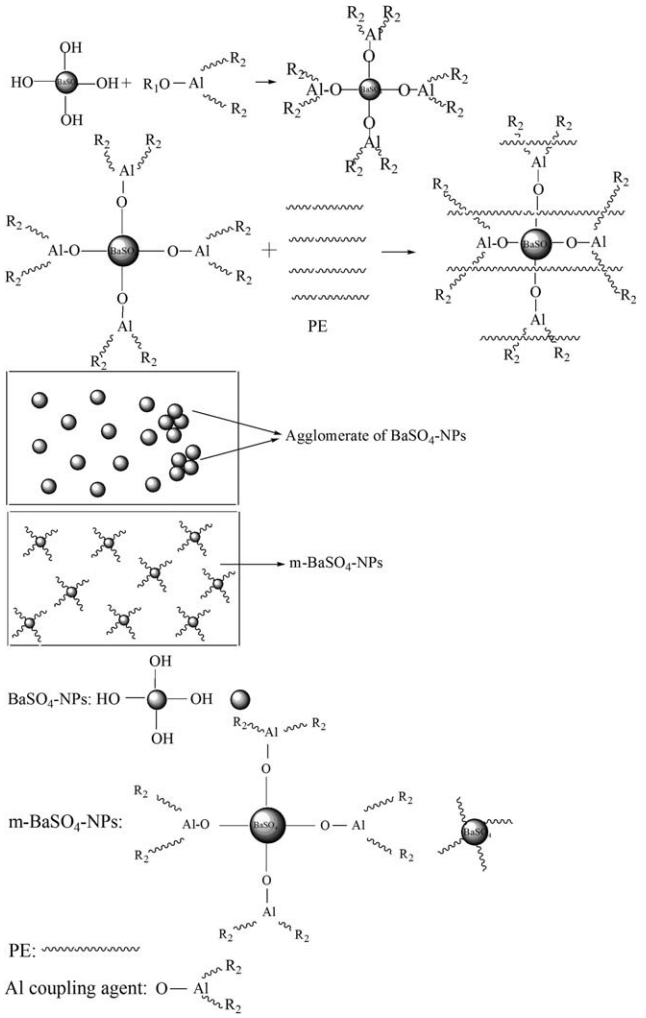

Scheme 1. Schematic representation of the surface modification of $BaSO_4$-NPs and their dispersion in the PE matrix.

disadvantages of the yield point and stress concentration in the PE matrix that worsen the mechanical properties.

DSC studies of nonisothermal crystallization and melting behavior were performed to investigate the influence of phase morphology on the crystallization of PE in the composites. Figure 5(a) shows the heating curves of PE, 20 wt % $BaSO_4$-NPs/PE, and 20 wt % m-$BaSO_4$-NPs/PE nanocomposites. The melting temperatures (T_ms) of the nanocomposites remained approximately the same as that of the PE matrix, suggesting that T_m was not significantly affected by the addition of the reinforcement particles. However, the crystallization temperatures (T_cs) of PE and the 20 wt % $BaSO_4$-NPs/PE nanocomposite were different. Figure 5(b) shows the cooling curves of PE, 20 wt % $BaSO_4$-NPs/PE, and 20 wt % m-$BaSO_4$-NPs/PE nanocomposites. The 20 wt % m-$BaSO_4$-NPs/PE nanocomposites exhibited the highest T_c of 115.7°C, several degrees higher than that of PE (111.4°C). Based on the above results, we hypothesize that the crystallinity% of PE was accelerated by the addition of $BaSO_4$-NPs. A possible explanation is that $BaSO_4$-NPs, with their enormous surface area, acted as nucleating agents for PE crystallinity%. In this way, the well-dispersed m-$BaSO_4$-NPs in the PE matrix were beneficial to the increase in the crystallinity% rate of PE.

Figure 6 shows the TG curves of PE, 20 wt % $BaSO_4$-NPs/PE, and 20 wt % m-$BaSO_4$-NPs/PE nanocomposites. The initial decomposing temperature (T_{di}), which is defined as the temperature at which the weight loss of the sample is 10%, the maximum decomposing rate temperature (T_{max}), and residues at 800°C can be determined from Figure 6. The T_{di} of PE was 409°C, while the nanocomposites had higher T_{di}s than PE by 12°C. The T_{max} of PE was 482°C. We found that the nanocomposites displayed higher thermal stability than the pure PE. The 20 wt % m-$BaSO_4$-NPs/PE nanocomposite exhibited the highest T_{max} value of 519°C. However, the T_{max} value of 20 wt % $BaSO_4$-NPs/PE nanocomposites displayed a decreased value

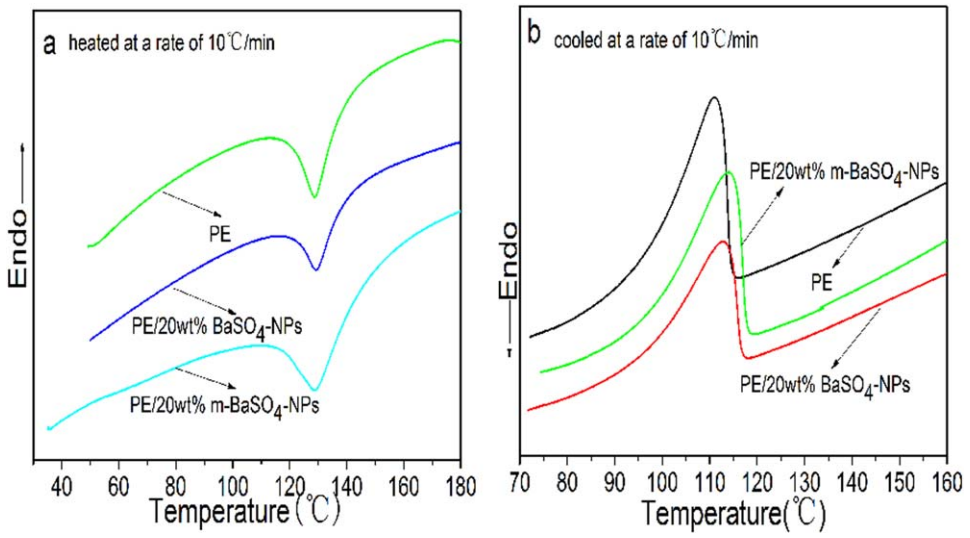

Figure 5. DSC (a) heating and (b) cooling scanning curves for PE, 20 wt % $BaSO_4$-NPs/PE, and 20 wt % m-$BaSO_4$-NPs/PE nanocomposites. [Color figure can be viewed in the online issue, which is available at wileyonlinelibrary.com.]

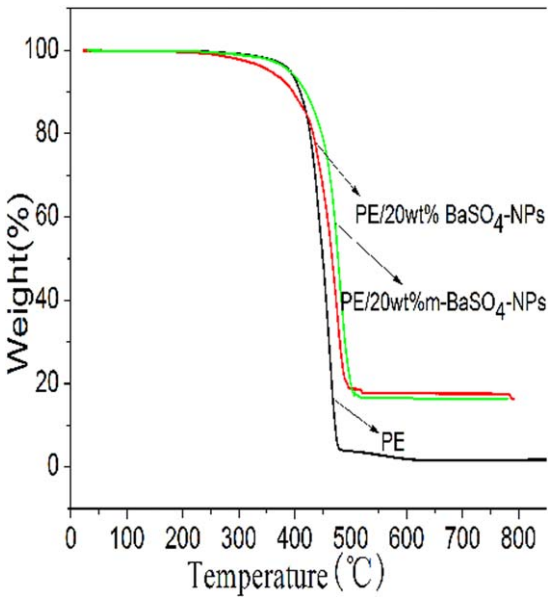

Figure 6. TG curves for PE, 20 wt % $BaSO_4$-NPs/PE, and 20 wt % m-$BaSO_4$-NPs/PE nanocomposites. [Color figure can be viewed in the online issue, which is available at wileyonlinelibrary.com.]

of 496°C. In summary, for the Al coupling agent-modified $BaSO_4$-NPs, the agglomeration tendency in the PE matrix was reduced, while the thermal stability of the nanocomposites was improved. In addition, the composites had more residues at 800°C than pure PE. The additional residues were related to the undecomposed $BaSO_4$-NPs within the range of temperatures tested.

Figure 7 shows the mechanical properties of different contents of Al coupling agent on the 20 wt % m-$BaSO_4$-NPs/PE nanocomposites. The presence of m-$BaSO_4$-NPs led to an increase in tensile strength and elongation at break in comparison to the $BaSO_4$-NPs. At Al coupling agent contents of 0.0, 0.5, 1.0, 1.5, and 3.0 wt %, the tensile strength was 10.25, 11.32, 11.87, 11.73, and 11.58 MPa, respectively, and the elongation at break was 54.32%, 65.32%, 67.78%, 66.67%, and 66.57%, respectively.

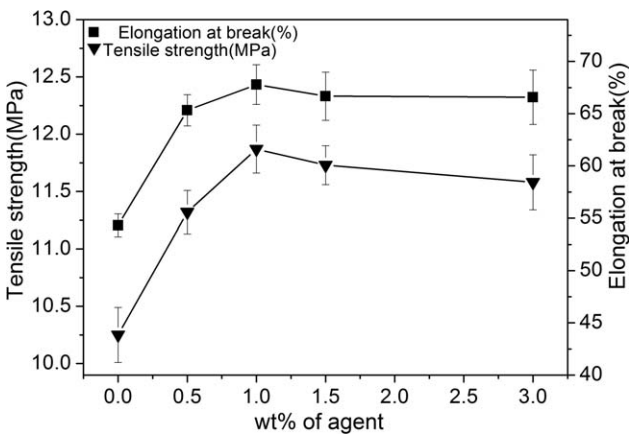

Figure 7. Tensile properties of 20 wt % m-$BaSO_4$-NPs/PE nanocomposites.

The tensile strength and elongation at break initially displayed an upward trend, which then decreased. The Al coupling agent also demonstrated some effect on the mechanical performance of the nanocomposites. At 1.0 wt % Al coupling agent, the tensile strength of the 20 wt % m-$BaSO_4$-NPs/PE nanocomposites increased by approximately 15.8% relative to the composites reinforced with unmodified $BaSO_4$-NPs, and the elongation at break increased by ~24.8%. A slight decrease was observed for 1.5 and 3.0 wt % Al coupling agent. The Al coupling agent content of 1.0 wt % was the best concentration, yielding the best particle dispersion and interfacial adhesion between the PE matrix and $BaSO_4$-NPs. Micro-structural analysis (Figure 4 for example) suggested that the improvement in mechanical strength and ductility was as a result of the more uniform dispersion of the NPs in the PE matrix after surface modification by the Al coupling agent.

According to the YY/T0681.1-2009 standard, the relationship between test time and shelf-life of PE/20 wt% m-$BaSO_4$-NPs nanocomposites was as follows:

$$\mathrm{TIME}_{T1} = \mathrm{TIME}_{RT} / Q_{10}^{(T_1 - T_{RT})/10}$$

T_1 is the accelerated aging temperature, T_{RT} is the ambient temperature, Q_{10} is the reaction rate constant, TIME_{RT} is the shelf-life, and TIME_{T1} is the test time ($T_1 = 90°C$, $T_{RT} = 37°C$, $Q_{10} = 2$, and $\mathrm{TIME}_{RT} = 520$ weeks). Therefore:

$$\mathrm{TIME}_{T1} = 520 \text{ weeks} / 2^{(90-37)10} = 13.2 \text{ weeks}.$$

From this formula we determined that the 13.2 weeks during the accelerated aging experiments at 90°C was equivalent to a shelf-life of 520 weeks at 37°C. Figure 8 shows the tensile properties of 20 wt % m-$BaSO_4$-NPs/PE nanocomposites with different contents of Al coupling agent after accelerated-aging experiments. The tensile strength and elongation at break decreased slightly after accelerated aging. The tensile strength of nanocomposites only decreased 5–15%, and elongation at break decreased 12–15%. However, the mechanical properties of the nanocomposites after accelerated aging were still able to satisfy the demands of clinical application. Therefore, such devices can be used for over 10 years.

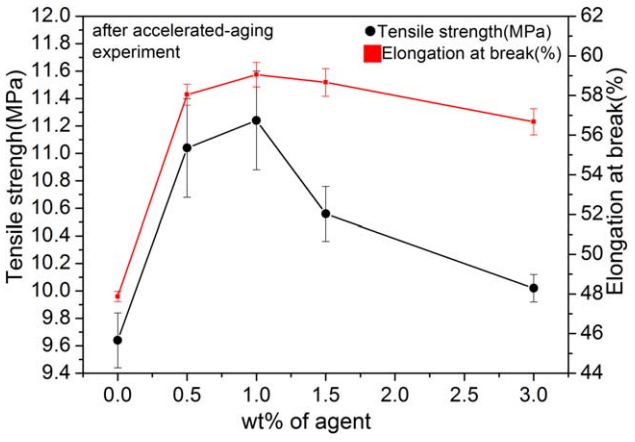

Figure 8. Tensile properties of 20 wt % m-$BaSO_4$-NPs/PE nanocomposites after accelerated-aging experiments. [Color figure can be viewed in the online issue, which is available at wileyonlinelibrary.com.]

CONCLUSION

Surface modification created bonding forces between polymer chains and m-$BaSO_4$-NPs. Al coupling agent surface-modified $BaSO_4$-NPs displayed enhanced properties compared to unmodified $BaSO_4$-NPs in terms of nanoscale dispersion in the PE matrix and the interfacial bonding between PE and the nanoparticles. The T_m of 20 wt% m-$BaSO_4$-NPs/PE nanocomposites was ~129°C. The T_c of the nanocomposites was 4.3°C greater than PE (111.4°C), and they also had the highest T_{max} of 519°C. When the surface of $BaSO_4$-NPs was modified by 1.0 wt % Al coupling agent, the tensile strength of the 20 wt % m-$BaSO_4$-NPs/PE nanocomposite increased approximately 15.8% relative to the unmodified $BaSO_4$-NPs reinforced nanocomposite, and the elongation at break increased by about 24.8%. After accelerated-aging experiments, the tensile strength of the nanocomposites only decreased 5–15%.

ACKNOWLEDGMENTS

This work was financially supported by Natural Science Foundation of China (Grant No. 51371126) and the Science and Technology Plan Project of Binhai new area in Tianjin (Grant No.2012-BK120024).

REFERENCES

1. Cao, B. M.; Xi, T. F.; Zheng, Y. D.; Yang, L. F.; Zheng, Q. *Chin. Sci. Bull.* **2009**, *54*, 3160.
2. Vanita, S.; Neelam, A.; Ravinder, K.; Neelam, C.; Pallab, R.; Anil, G. *Contraception* **2008**, *78*, 315.
3. Liang, J. Y.; Li, Y.; Gu, X.; Gao, Y. L.; Liu, J. P. *Contraception* **2008**, *77*, 299.
4. Yang, Z. H.; Xie, C. S.; Xiang, H.; Feng, J.Q.; Xia, X.P.; Cai, S.Z.; *Colloids Surf. B Biointerfaces* **2009**, *69*, 276.
5. Xia, X. P.; Xie, C. S.; Zhu, C. H.; Cai, S. Z.; Yang, X. L. *Fertil. Steril.* **2007**, *88*, 472.
6. Colbeaux, A.; Fenouillot, F.; Gerard, J. F.; Taha, M.; Wautier, H. *Polym. Int.* **2005**, *54*, 692.
7. Hu, G. S.; Wang, B. B.; Zhou, X. M. *Polym. Int.* **2005**, *54*, 316.
8. Zeng, X. F.; Wang, W. Y.; Wang, G. Q.; Chen, J. F. *J. Mater. Sci.* **2008**, *43*, 3505.
9. Chanunpanich, N.; Ulman, A.; Strzhemechny, Y. M.; Schwarz, S. A.; Dormicik, J.; Janke, A.; Braun, H. G.; Kratzmuller, T. *Polym. Int.* **2003**, *52*, 172.
10. Yu, Z. Z.; Ou, Y. C.; Hu, G. H. *J. Appl. Polym. Sci.* **1998**, *69*, 1711.
11. Li, Z.; Guo, S. Y.; Song, W. T.; Hou, B. *J. Mater. Sci.* **2003**, *38*, 1793.
12. Qu, M. H.; Wang, Y. Z.; Liu, Y.; Ge, X. G.; Wang, D. Y.; Wang, C. *J. Appl. Polym. Sci.* **2006**, *102*, 564.
13. Bianchi, F.; Lazzeri, A.; Pracella, M.; D'Aquino, A.; Ligeri, G. *Macromol. Seem.* **2004**, *218*, 191.
14. Wang, K.; Wu, J. S.; Ye, L. *Compos. Part A Appl.* **2003**, *34*, 1199.
15. Xu, Y.; Zhang, X. Z.; Zhou, C. X.; Wu, W. S.; Shi, L. Y.; Yang, B. *J. Polym. Sci. Eng.* **2007**, *23*, 144.
16. Wang, K.; Wu, J. S.; Zeng, H. M. *J. Eur. Polym.* **2003**, *39*, 1647.
17. Ye, Q. M.; Wang, L.; Liu, J.; Lin, J. H.; Deng, M. *J. Mineral. Petrol.* **2005**, 03.
18. Shen, Y. H.; Li, C. N.; Zhu, X. M.; Xie, A. J.; Qiu, L. G.; Zhu, J. M. *J. Chem. Sci.* **2007**,*119*, 319.